

Diversity of multiwavelength emission bumps in the GRB 100219A afterglow

J. Mao^{1,2,3,4}, D. Malesani⁵, P. D'Avanzo⁴, S. Covino⁴, S. Li^{2,3}, P. Jakobsson⁶, and J. M. Bai^{2,3}

¹ Space Science Division, Korea Astronomy and Space Science Institute, 776, Daedeokdae-ro, Yuseong-gu, Daejeon, 305-348, Republic of Korea
e-mail: jirongmao@mail.ynao.ac.cn

² Yunnan Astronomical Observatory, Chinese Academy of Sciences, Kunming, Yunnan Province, 650011, China

³ Key Laboratory for the Structure and Evolution of Celestial Objects, Chinese Academy of Sciences, Kunming, Yunnan Province, 650011, China

⁴ INAF-Osservatorio Astronomico di Brera, Via Bianchi 46, I-23807, Merate (LC), Italy

⁵ Dark Cosmology Centre, Niels Bohr Institute, University of Copenhagen, Juliane Maries Vej 30, 2100, Copenhagen, Denmark

⁶ Centre for Astrophysics and Cosmology, Science Institute, University of Iceland, Dunhagi 5, 107 Reykjavik, Iceland

Received ?, ?, ?; accepted ?, ?, ?

ABSTRACT

Context. Multi-wavelength observations of gamma-ray burst (GRB) afterglows provide important information about the activity of their central engines and their environments. In particular, the short timescale variability, such as bumps and/or rebrightening features visible in the multi-wavelength light curves, is still poorly understood.

Aims. We analyze the multi-wavelength observations of the GRB 100219A afterglow at redshift 4.7. In particular, we attempt to identify the physical origin of the late achromatic flares/bumps detected in the X-ray and optical bands.

Methods. We present ground-based optical photometric data and *Swift* X-ray observations on GRB 100219A. We analyzed the temporal behavior of the X-ray and optical light curves, as well as the X-ray spectra.

Results. The early flares in the X-ray and optical light curves peak simultaneously at about 1000 s after the burst trigger, while late achromatic bumps in the X-ray and optical bands appear at about 2×10^4 s after the burst trigger. These are uncommon features in the afterglow phenomenology. Considering the temporal and spectral properties, we argue that both optical and X-ray emissions come from the same mechanism. The late flares/bumps may be produced by late internal shocks from long-lasting activity of the central engine. An off-axis origin for a structured jet model is also discussed to interpret the bump shapes. The early optical bump can be interpreted as the afterglow onset, while the early X-ray flare could be caused by the internal activity. GRB 100219A exploded in a dense environment as revealed by the strong attenuation of X-ray emission and the optical-to-X-ray spectral energy distribution.

Key words. gamma rays: bursts – X-rays: general – ISM: dust, extinction – shock waves

1. Introduction

Gamma-ray bursts (GRBs) are detected by high-energy observational satellites. Ground-based telescopes can be subsequently alerted and perform follow-up observations. The accurate positions delivered by the *Swift* satellite provide an excellent opportunity for multi-wavelength observations. The analysis of GRB light curves can provide plenty of information about the central engine and the surrounding environment. A canonical shape has been identified for the X-ray light curves (Nousek et al. 2006; Zhang et al. 2006), as obtained by the *Swift* X-ray Telescope (XRT). In the optical band, following the alert by the *Swift* Burst Alert Telescope (BAT), ground-based follow-up observations carried out by robotic telescopes increased the number of well-sampled optical light curves significantly (see, e.g., Melandri et al. 2008; Klotz et al. 2009; Rykoff et al. 2009; Cenko et al. 2009). Apparently, these light curves present different temporal behaviors. It is hard to identify a uniform characterization for them. An attempt to classify the temporal properties has been

made by Melandri et al. (2008). Rykoff et al. (2009) attempted to find commonalities within a sample of optical light curves, finding that the external forward shock is a possible origin for the overall optical emission. Panaitescu et al. (2006) have studied in detail the decay of light curves both in the X-ray and optical bands from a theoretical point of view. Chromatic breaks identified by comparing optical and X-ray light curves indicate that most likely the optical and X-ray emissions arise from a different origin.

While light curves generically decay in time, in several cases rebrightenings or bumps are observed in the X-ray or optical bands. These features call for a more detailed investigation of the physics of GRB and afterglow. However, the situation is quite complicated. Most rebrightenings are only observed in the X-ray band. Some early X-ray bumps, usually called X-ray flares, have no corresponding optical features (see the statistics by Melandri et al. 2008 and Rykoff et al. 2009, as well as Uehara et al. 2010 for the individual cases of GRB 071112C and GRB 080506).

In contrast, but less frequently, a rebrightening feature may be seen in the optical but not in the X-ray band (e.g. GRB 050721; Antonelli et al. 2006). Some GRBs with both X-ray and optical bumps shown before 1000 s in the observer's frame have been identified: GRB 060418 and GRB 060607A (Molinari et al. 2007), GRB 060904B (Klotz et al. 2008) and GRB 071031 (Krühler et al. 2009). The X-ray flare and optical bump of GRB 060418 have the same peak time. However, it is likely that the X-ray flare has an internal origin while the optical bump is the result of external shock onset (see the optical statistics from Oates et al. 2008). The optical bump and giant X-ray flare of GRB 060904B are clearly chromatic. The optical rising and X-ray flare of GRB 071031 are not exactly simultaneous, but their observed correlation suggests a common origin caused by late central engine activity.

More importantly, it is worth noting that GRBs with late bumps/rebrightenings shown after 10^3 – 10^4 s in the observer's frame are very rare. We mention that the X-ray light curves of GRB 050502B, GRB 050724, GRB 050904, GRB 060413, GRB 060906, and GRB 070311 have similar late bump/flare/wiggle features. Some of them have been identified as late X-ray flares (Curran et al. 2008; Bernardini et al. 2011). It is rare, however, to have well-sampled, complete optical data at the time corresponding to the late X-ray bumps (see, e.g., Afonso et al. 2011). A broad, late optical rebrightening was found by Mundell et al. (2007) for GRB 061007, but no corresponding bump was seen in the X-ray band. The late-observed optical emission of GRB 050724 is likely related to the X-ray flare peaking at 41.8 ks, but the evidence for an optical rebrightening is not conclusive (Malesani et al. 2007). GRB 070311 is one case with relatively clear evidence of late bumps in both the X-ray and optical bands (Guidorzi et al. 2007), with comparable, although not simultaneous, peak times. The most interesting case is GRB 071010A, for which a late rebrightening feature was identified at 0.6 day after the trigger, visible simultaneously in both the optical/NIR and X-ray bands (Covino et al. 2008).

Several mechanisms responsible for the X-ray and optical bumps presented in GRB light curves have been proposed. Kumar et al. (2008a, b) suggested a model for the early flares powered by accretion of fall-back matter from the progenitor star. In general, early and late X-ray flares may have an internal origin although the detailed physics is unclear (Chincarini et al. 2010; Bernardini et al. 2011). An early rising of the optical light curve can be sometimes caused by the onset of forward shock (Oates et al. 2009), another discussion was given by Melandri et al. (2010). Some late optical bumps are interpreted by the external shock model. For example, the optical rebrightening feature of GRB 021004 seen at 0.1 days after the burst (Holland et al. 2003) can be explained by the interaction with a clumpy ambient (Lazzati et al. 2002; but see also Nakar et al. 2003). An early rising feature around 1000 s and a later rebrightening behavior after 10^4 – 10^5 s can be described by the standard reverse-forward shock model as well (Zhang et al. 2003, Fan et al. 2005). However, for the short burst GRB 060313, the wiggles shown at about 10^4 s have been proposed to be the result of late-time central engine activity (Romig et al. 2006). To explain the late rebrightening of GRB 070311 (Guidorzi et al. 2007), refreshed shocks were proposed (Rees & Mészáros 1998). The achromatic rebrightening feature of GRB 071010A may be produced by an episode of discrete energy injection (Covino et al. 2008).

In this paper, we analyze the X-ray and optical light curves of GRB 100219A. We report data taken from the 2.4-m telescope at Gao-Mei-Gu (GMG) and from the Nordic Optical Telescope (NOT), with the former providing most of the data. The opti-

cal light curve shows a clear rebrightening around 2×10^4 s after the GRB trigger. A simultaneous X-ray temporal wiggle/small bump is also detected. Thus, the late achromatic bumps of GRB 100219A provide us with an excellent opportunity to investigate the origin of the bumps/flares in the different observational bands in more detail.

We describe all observations of GRB 100219A in Section 2. The GMG and NOT telescopes have similar mirror size and detectors. Being located at roughly the same latitude in the Northern hemisphere, paired together they provide an excellent chance for continuing observations of GRB afterglows. In Section 3 we compare the optical light curves with the X-ray data, and we identify achromatic bumps in the X-ray and optical light curves. We also use the optical-to-X-ray spectral energy distribution (SED), aiming at investigating whether the late optical and X-ray bumps come from the same mechanism. The discussion about the possible physical origin is presented in Section 4. In Section 5, our conclusions are summarized.

Throughout the paper, we adopt the convention $F_\nu(t, \nu) \propto t^{-\alpha} \nu^{-\beta}$ and cosmological parameters $H_0 = 70 \text{ km s}^{-1} \text{ Mpc}^{-1}$, $\Omega_m = 0.3$ and $\Omega_\Lambda = 0.7$.

2. Observations

2.1. Swift observations

GRB 100219A was discovered by *Swift*/BAT on 2010 February 19 at $T_0 = 15:15:46$ UT (Rowlinson et al. 2010). BAT observations (Baumgartner et al. 2010) reveal that the prompt light curve has a roughly triangular shape peak starting at $T_0 - 10$ s, the peak time is at about $T_0 + 30$ s, and the burst ends at $T_0 + 50$ s. The pulse duration is $T_{90} = 18.8 \pm 5.0$ s. The BAT time-averaged spectrum can be fitted by a simple power-law model, the power-law index being $\Gamma = 1.34 \pm 0.25$. The fluence in the 15–150 keV band is $(3.7 \pm 0.6) \times 10^{-7} \text{ erg cm}^{-2}$. *Swift*/XRT began observing the location of GRB 100219A 178.5 s after the BAT trigger (Rowlinson 2010). *Swift*/UVOT began observations starting 161 s after the BAT trigger as well (Holland, Kuin & Rowlinson 2010; Holland & Rowlinson 2010), leading to the detection of a variable object.

2.2. GMG and NOT optical observations

Since January 2009, a program of GRB follow-up has been carried out with the 2.4-m telescope at Lijiang station of Yunnan Astronomical Observatory, CAS (longitude = $100^\circ 01' 51''$ E, latitude = $26^\circ 42' 32''$ N, altitude = 3193 m). The telescope is equipped with standard Johnson *UBVRI* filters and a 1340×1300 pixels CCD with a pixel scale of $0.214''/\text{pixel}$. The field of view is $4' 48'' \times 4' 40''$. The GMG telescope began observing the GRB 100219A afterglow on 2010 February 19 at 15:30:15 UT, about 15 minutes after the *Swift*/BAT trigger, taking a sequence of *R*-band observations. The burst location was observed again on 2010 February 21, starting at 15:14:30 UT, about 2 days after the trigger.

After correcting the raw images with bias and flat fields, we used the Source Extractor software (SExtractor; Bertin & Arnouts 1996) to accurately determine the GRB position. We successfully detected both the GRB optical afterglow and a nearby faint object, located $3.1''$ northeast of the afterglow position (Fig. 1, upper panel). Because the seeing of the GMG observation was poor ($1.8''$), we were unable to separate the two objects at the beginning of our observations. As the afterglow was fading, we were able to clearly identify the two objects in the later images. We computed the afterglow position using

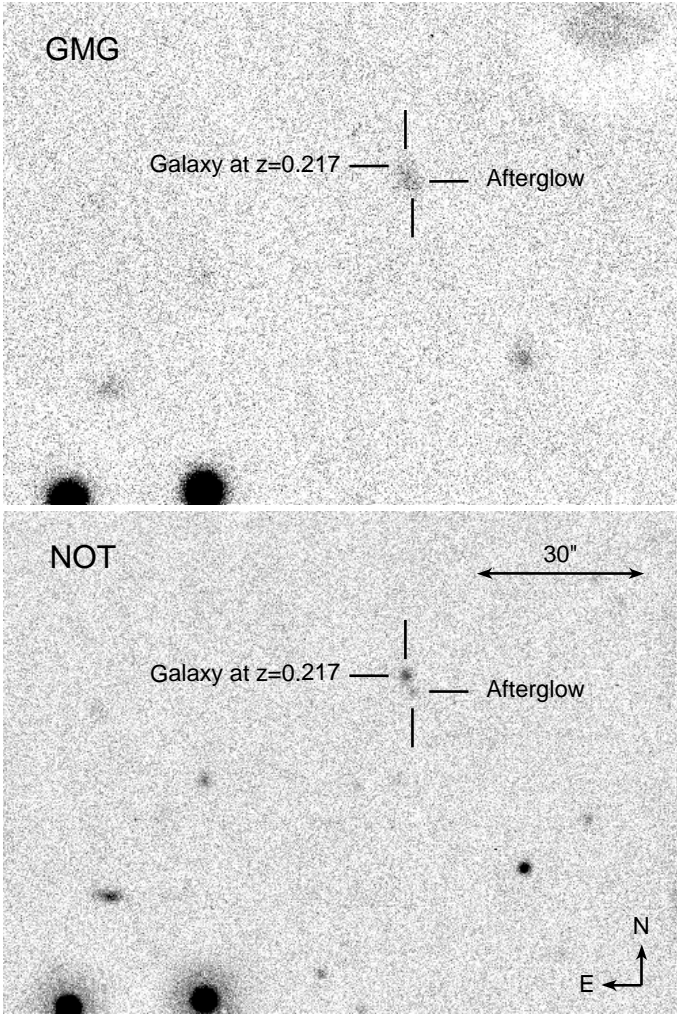


Fig. 1. Field and optical counterpart of GRB 100219A as observed by the NOT (lower panel) and by the GMG (upper panel). The galaxy at $z = 0.217$ is not related to the GRB.

the USNO catalog as reference. With the $0.15''$ uncertainty of the USNO catalog (Zacharias 1997), the optical afterglow position of GRB 100219A is located at $RA = 10^h 16^m 48.54^s$, $Dec = -12^\circ 33' 59.5''$ with an error of $0.34''$ in the R -band images. This position is fully consistent with the outcome of the NOT observation (Jakobsson et al. 2010) and the enhanced *Swift*/XRT position (Evans et al. 2010).

In order to separate the two objects, we first used DAOPHOT (Stetson 1987) to obtain the average point spread function (PSF) in each image. Then, we used this PSF model to match the afterglow and nearby faint source. Both sources are pointlike, and with this procedure we were able to obtain accurate magnitudes of the optical afterglow.

The 2.5-m NOT (longitude = $17^\circ 53' 06.3''$ W, latitude = $28^\circ 45' 26.2''$ N, altitude = 2382 m) began observing GRB 100219A starting on 2010 Feb 20, at 00:11:58.5 UT, about 9 hr after the trigger. After correcting the raw images for the effect of CCD flat and bias, we carried out the R -band photometry using DAOPHOT through the selected unsaturated objects in the images to be consistent with the GMG observation. Since the NOT observations were carried out under better seeing conditions ($\sim 1.4''$), the GRB afterglow and the nearby faint object are resolved.

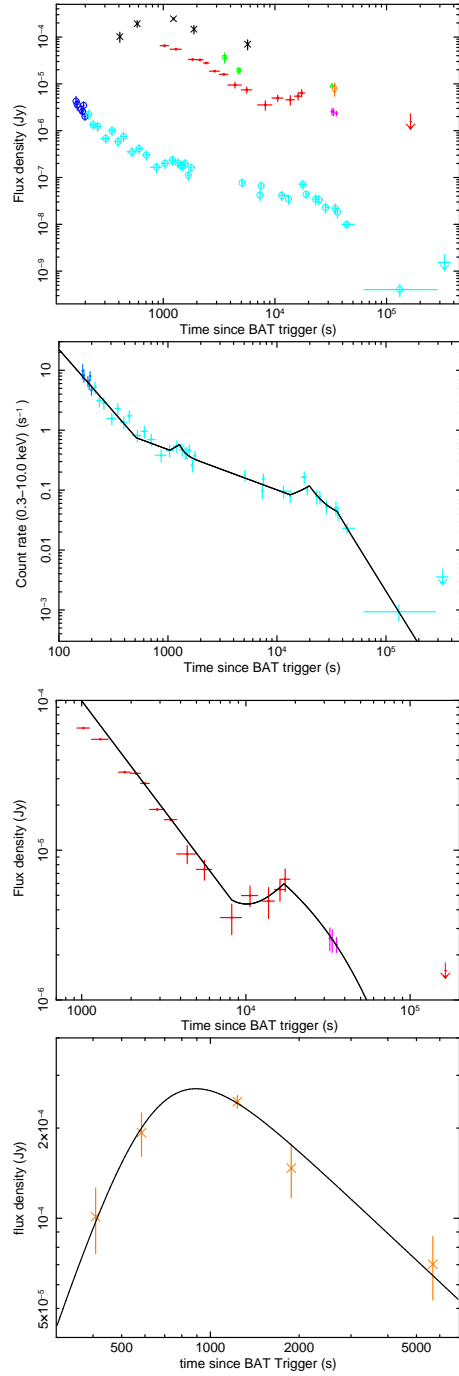


Fig. 2. Panel 1: multi-wavelength light curves of the GRB 100219A afterglow. The X-ray light curve at 1 keV is represented by empty circles (dark blue: WT data; light blue: PC data). The values in the plot are 10 times lower than the real ones for presentation purposes. The GMG and NOT R -band data are denoted by dots (red: GMG data; pink: NOT data). The I -band datum from the NOT is indicated by a diamond (orange color). The GAO 150 cm R_C and I_C band observations are denoted by empty squares (green color). The Akeno and Okayama MITSuME optical I_C -band observations are denoted by crosses (black color). The GROND i' -band observation is marked with a triangle (green color). Panel 2: the whole X-ray light curve fitting from about 100 s to 4×10^4 s after the burst trigger and two X-ray bumps are included in the fitting. Panel 3: the fitting of optical R -band light curve of GMG and NOT observations from about 1000 s to 2×10^5 s after the burst trigger and the late optical bump is included. Panel 4: the fitting of optical I_C band light curve of MITSuME observation from about 400 s to 6000 s after the burst trigger and the early optical bump is clearly shown. The solid line in each panel is the light curve fitting result.

To obtain absolute flux measurements, the standard star field SA 105815 from the Landolt (1992) catalog was observed for photometric calibration. We selected some non-saturated objects in the images as comparison stars when we performed the photometric analysis; the magnitude measurements of GMG and NOT are fully consistent. The final results of the photometry are listed in detail in Table 1. We present the images from the NOT and GMG in Fig. 1.

2.3. Other optical observations and spectral redshift

The optical afterglow of GRB 100219A was also detected by other ground-based telescopes. Results of their photometric observations have been reported by Kuroda et al. (2010) at 104 s after the trigger (MITSuME telescope of the Akeno Observatory and Okayama Astrophysical Observatory), by Kinugasa et al. (2010) at 0.9 hr after the trigger (GAO observations), and later by Krühler et al. (2010) at 8.7 hr after the trigger (GROND observations). We collect these results in Table 2.

Spectral measurements were reported by Groot et al. (2010), Cenko et al. (2010), and de Ugarte Postigo et al. (2010). From the detection of a series of absorption lines, the redshift was estimated to be $z = 4.6667 \pm 0.0005$ through VLT/X-shooter spectroscopy (de Ugarte Postigo et al. 2010; Thöne et al. 2011). The nearby object, with a redshift of 0.217 (Cenko et al. 2010; Thöne et al. 2011), is a galaxy not related to the GRB (as initially suggested by Bloom & Nugent 2010).

3. Results

From *Swift*/BAT observation, the fluence of GRB 100219A in the 15–150 keV band is $(3.7 \pm 0.6) \times 10^{-7}$ erg cm⁻². With this fluence, the isotropic energy detected by BAT is $E_{\text{iso,BAT}} \sim 1.4 \times 10^{52}$ erg. On the other hand, from the scaling relation of Sakamoto et al. (2009), we can calculate the peak energy in the observer frame $\log(E_{\text{peak}}/\text{keV}) = 3.258 - 0.829\Gamma$ where $\Gamma = 1.34$ is the photon index of the spectrum fitted with a single power-law. The peak energy ~ 140 keV is therefore likely to be above the spectral range covered by BAT, indicating that the bolometric energy can be significantly higher. The peak energy in the rest frame is $E_{\text{peak,rest}} = E_{\text{peak}} \times (1 + z) \sim 800$ keV. Assuming that GRB 100219A obeys the $E_{\text{peak,i}} - E_{\text{iso}}$ relation (“Amati” relation, Amati et al. 2002, 2006), we predict that the prompt emission of GRB 100219A is about $E_{\text{iso}} \approx 7.7 \times 10^{53}$ erg.

3.1. Light curve features

In order to analyze the GRB 100219A multi-wavelength observations and reveal the involved physics, we also considered the X-ray data taken by *Swift*. We used the XRT light curve of GRB 100219A from the automatic online repository¹. The flux can be obtained by transforming the count rate with the conversion factor deduced from the X-ray spectrum. The adopted procedures are described in detail by Evans et al. (2007, 2009). The X-ray light curve shows overall the canonical shape (Nousek et al. 2006). However, we note two small bumps/wiggles, at about 10^3 and 2×10^4 s.

We converted the GMG and NOT observations from *R*-band magnitude to flux density. The results of MITSuME, GAO, and GROND are also reported. The optical light curve shows a brightening as indicated by the MITSuME *I*_C-band observation, peaking at about 1000 s. The GMG observations subsequently

reveal a clearly fading phase from about 10^3 to 10^4 s. After the decay, the optical light curve shows a clear rebrightening, peaking at about 2×10^4 s. The multi-wavelength light curves are plotted in Fig. 2. We note that the early and late bumps shown in the X-ray and optical light curves are simultaneous.

In order to investigate the temporal behavior of the GRB 100219A afterglow in more detail, we performed a fit to the X-ray and optical light curves. In the fitting process, we focused on the shapes of the flares/bumps in addition to the general light curves. The overall X-ray light curve can be fitted by a double-broken power-law. The decay index of the initial steep phase is 2.07 ± 0.29 . At 635 ± 134 s, it turns into a relatively flat stage with a decay index of 0.66 ± 0.06 . After that, at $(3.5 \pm 1.0) \times 10^4$ s, the light curve turns again steeply decays with an index of 2.93 ± 0.29 . The two bumps apparent in the X-ray light curve were fitted with the same fitting procedure. Chincarini et al. (2007) fitted the X-ray flares with a Gaussian profile and with the prompt pulse profile introduced by Norris et al. (2005), showing that the latter provides a better fit. We adopted the burst model, a profile with a linear rising, and an exponential decay². We obtained for the first flare a peak time of $t_p = 1272 \pm 170$ s and for the second flare a peak time of $t_p = (1.67 \pm 0.48) \times 10^4$ s. The decay timescales are 157 ± 237 s and 4365 ± 6948 s, respectively. The fit has $\chi^2/\text{dof} = 23.7/33$.

The overall optical light curve obtained by GMG data after 2000 s can be fitted by a power-law with decay index 1.45 ± 0.04 . After the time 8203 ± 2442 s, the optical light curve shows a rebrightening feature. With the burst fitting model, the rebrightening peaks at the time $(1.71 \pm 0.21) \times 10^4$ s and the decay duration is $(2.04 \pm 0.67) \times 10^4$ s. The fit has $\chi^2/\text{dof} = 17.0/13$. The F-value of 1.22 and P-value of 0.68 indicate that our fitting is acceptable.

Furthermore, as can be seen in Fig. 2, an early rebrightening is shown by the *I*_C-band light curve provided by Kuroda et al. (2010). We fitted the *I*_C-band light curve using the function $F(t) = F_0 / [(t/t_b)^{\alpha_r} + (t/t_b)^{\alpha_d}]^{1/k}$ (Molinari et al. 2007), where t_b is break time, α_r (α_d) is the rise (decay) slope, k is the smoothness parameter, and F_0 is normalization. After the fitting, we obtained $t_b = 660 \pm 120$ s, $\alpha_r = -3.0 \pm 1.3$, $\alpha_d = 0.90 \pm 0.20$, $F_0 = (4.68 \pm 0.46) \times 10^{-4}$ Jy, and we fixed the parameter $k = 1$. The fit has $\chi^2/\text{dof} = 5.85/5$. Therefore, the peak time of the bump is $t_p = t_b(-\alpha_r/\alpha_d)^{1/[k(\alpha_d - \alpha_r)]} = 900 \pm 470$ s. We note that these *I*_C-band data are selected from public GCN circular and we do not have any accurate calibration.

Finally, we plot the fit results in Fig. 2 as well. All errors are at 1σ confidence level³. Our fits quantitatively confirm that the early and late bumps visible in the X-ray and optical light curves peak simultaneously.

3.2. Spectral analysis

Both windowed timing (WT) and photon counting (PC) data of GRB 100219A have been collected during the *Swift*/XRT observation. Here, we consider the PC mode data, which are simultaneous to our optical data. We downloaded the XRT level 2 cleaned event files and use `xselect` task to extract the spec-

² $F(t) \propto (t - t_s)/(t_p - t_s)$ if $t < t_p$ and $F(t) \propto \exp(-(t - t_p)/dt)$ if $t > t_p$, where t_s is the start time, t_p is the peak time and dt is the duration. This profile was selected by Perri et al. (2007) to describe the X-ray flares of GRB 050730.

³ At the beginning of the *R*-band light curve, the first two data points (before 1200 s) show a deviation from the fitting line. These two data points probably mark the end of the early rebrightening phase peaking at about 1000 s that are clearly visible in the *I*-band light curve.

¹ http://www.swift.ac.uk/xrt_curves/00412982/

Table 1. GMG and NOT observations of GRB 100219A in 2010. Data are not corrected for Galactic extinction.

Telescope	Date	Start time UT	Time since trigger (s)	Exp. time (s)	Magnitude	Filter	Seeing (")
GMG	19 Feb	15:31:22	936	180	19.13 ± 0.05	<i>R</i>	1.8
GMG	19 Feb	15:34:55	1149	300	19.32 ± 0.05	<i>R</i>	1.8
GMG	19 Feb	15:43:45	1679	300	19.87 ± 0.08	<i>R</i>	1.8
GMG	19 Feb	15:48:48	1882	300	19.89 ± 0.09	<i>R</i>	1.8
GMG	19 Feb	15:53:50	2284	300	20.06 ± 0.09	<i>R</i>	1.8
GMG	19 Feb	15:58:53	2587	600	20.49 ± 0.13	<i>R</i>	1.8
GMG	19 Feb	16:08:54	3188	600	20.66 ± 0.22	<i>R</i>	1.8
GMG	19 Feb	16:18:59	3793	1200	21.23 ± 0.16	<i>R</i>	1.8
GMG	19 Feb	16:38:58	4992	1200	21.49 ± 0.18	<i>R</i>	1.8
GMG	19 Feb	17:12:29	7003	2400	22.30 ± 0.29	<i>R</i>	1.8
GMG	19 Feb	17:52:24	9398	2400	21.93 ± 0.19	<i>R</i>	1.8
GMG	19 Feb	18:44:43	12537	2400	22.02 ± 0.29	<i>R</i>	1.8
GMG	19 Feb	19:24:42	14936	2400	21.83 ± 0.18	<i>R</i>	1.8
GMG	19 Feb	20:04:40	17334	2400	21.66 ± 0.21	<i>R</i>	1.8
GMG	21 Feb	15:14:30	172784	2400	>23.18 (3 σ)	<i>R</i>	1.1
NOT	20 Feb	00:11:58	32172	600	22.64 ± 0.21	<i>R</i>	1.4
NOT	20 Feb	00:24:27	32921	600	22.67 ± 0.21	<i>R</i>	1.4
NOT	20 Feb	00:58:44	34978	600	22.75 ± 0.23	<i>R</i>	1.3
NOT	20 Feb	00:46:25	34239	300	21.31 ± 0.41	<i>I</i>	1.4

Table 2. Optical observations of GRB 100219A in 2010 taken from the GCN circulars. GROND started the observation at 00:30 UT.

Telescope	Date	Middle time	Magnitude	Filter	Reference
Akeno	19 Feb	15:22:34	18.5 ± 0.3	<i>I_C</i>	GCN 10440
Okayama	19 Feb	15:25:30	17.8 ± 0.2	<i>I_C</i>	GCN 10440
Okayama	19 Feb	15:36:21	17.5 ± 0.1	<i>I_C</i>	GCN 10440
Okayama	19 Feb	15:47:07	18.1 ± 0.3	<i>I_C</i>	GCN 10440
Okayama	19 Feb	16:50:40	18.9 ± 0.3	<i>I_C</i>	GCN 10440
GAO	19 Feb	16:15:24	20.5 ± 0.2	<i>R_C</i>	GCN 10452
GAO	19 Feb	16:34:45	19.6 ± 0.3	<i>I_C</i>	GCN 10452
GROND	20 Feb	about 00:50	21.5	<i>i'</i>	GCN 10439

trum. We used the response matrix file from the XRT standard calibration database and the arf file built by `xrtmkarf`. We extracted two spectra for two different time intervals, ranging from $T_0 + 212$ s to $T_0 + 1814$ s and from $T_0 + 5.0 \times 10^3$ s to $T_0 + 1.8 \times 10^5$ s, respectively. Each time interval includes one X-ray flare. First, we used Swift online repository⁴ (Evans et al. 2007, 2009) to fit the spectra using an absorbed power-law. We found a spectral index $\beta = 0.69^{+0.17}_{-0.12}$ and an intrinsic column density upper limit $N_H \sim 1.9 \times 10^{22} \text{ cm}^{-2}$ for the first spectrum (reduced $\chi^2/\text{dof} = 233.3/254$), and $\beta = 0.86^{+0.16}_{-0.26}$ and $N_H = 7.2^{+4.3}_{-4.7} \times 10^{22} \text{ cm}^{-2}$ for the second spectrum (reduced $\chi^2/\text{dof} = 166.0/186$). The Galactic column density is $N_H = 6.5 \times 10^{20} \text{ cm}^{-2}$.

To more thoroughly investigate the potentially large amount of absorption, we attempted another spectral fit. We fitted the same spectra as above with a broken power-law. For the first spectrum, we obtained $\beta_1 = -1.63 \pm 1.79$, $\beta_2 = 0.53 \pm 0.06$ with the peak energy $E_p = 0.60 \pm 0.11$ keV. For the second spectrum, we obtained $\beta_1 = -0.58 \pm 2.05$, $\beta_2 = 0.55 \pm 0.18$, and $E_p = 0.90 \pm 0.44$ keV. The low-energy spectral indices are poorly determined. The two fits have a reduced χ^2/dof of 35.2/37 and 12.9/9, respectively. All the spectral parameter errors are at 1 σ level.

Using the optical and X-ray fluxes, we also constructed the optical-to-X-ray SEDs shown in **Fig. 3**. The X-ray flux density was computed at 1 keV. Using the *R*-band measurements, we

obtained β_{OX} values of 0.27, 0.42, 0.35, and 0.41 at 8, 13, 17, and 35 ks after the burst trigger, respectively. These values are well below the limit for the definition of dark bursts first proposed by Jakobsson et al. (2004a). We note that at redshift $z = 4.7$, the *R*-band flux is strongly suppressed by the Ly α absorption. This is likely the main reason for the low value of β_{OX} . The *I*-band flux is not affected by Ly α blanketing, and using this flux we obtained $\beta_{\text{OX}} \sim 0.56$ around 3.4×10^4 s.

We compared the β_{OX} values with the X-ray spectral indices. The X-ray fits using a broken power-law are not consistent with the optical-to-X-ray SED. On the contrary, the X-ray spectral shape fitted with an absorbed power-law can be roughly extrapolated to the *I*-band flux level, indicating that the simple power-law model could fit both the X-ray and optical spectra. Therefore, the multi-wavelength data seem to require the presence of strong excess absorption in the X-ray spectra. We note that the *I*-band datum lies marginally below the extrapolation of the X-ray spectrum. This can be taken as an indication of moderate dust extinction associated with the absorbing matter that affects the optical (rest-frame UV) data. The SED results also suggest that the emission of GRB 100219A in both the X-ray and optical bands is coming from the same mechanism.

4. Discussion

As we have listed in Section 1, there are very few cases reported so far of late flares/bumps observed to peak simultaneously in the optical and X-ray bands (e.g. Covino et al. 2008 for

⁴ http://www.swift.ac.uk/xrt_spectra/00412982/

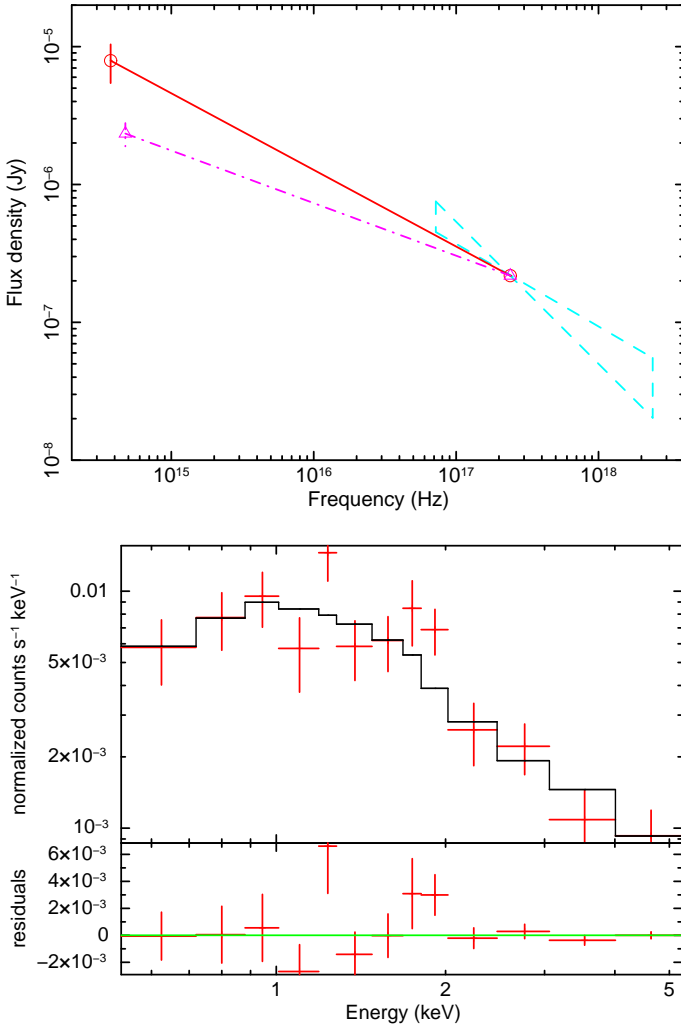


Fig. 3. Upper panel: the optical-to-X-ray spectral energy distribution of the afterglow of GRB 100219A is shown in the upper panel. The X-ray point corresponds to 1 keV. The values of β_{OX} relative to the I -band (unaffected by the $\text{Ly}\alpha$ blanketing) and R -band (affected by the $\text{Ly}\alpha$ blanketing) are 0.56 ($t = 34$ ks) and 0.41 ($t = 35$ ks), marked with a solid line and a dash-dotted line, respectively. The Galactic correction $E(B - V) = 0.08$ is used. Lower panel: fitting of the late X-ray spectrum with a broken power-law. The time interval is between 5.0×10^3 s and 1.8×10^5 s.

GRB 071010A). The rebrightening features in the optical and X-ray bands of GRB 071010A were suggested to originate from a discrete episode of energy injection. We presented the case of GRB 100219A, which provides another example of achromatic bumps.

If we assume that the early optical bump peaking at 895 s shown in I_C band light curve is originally from the onset of the forward shock (Oates et al. 2009), the Lorentz factor of the burst shock can be given by $\Gamma(t_{\text{peak}}) = 160[E_{\text{iso},53}(1+z)^3/n_0 t_{p,2}^3]^{1/8}$ from the estimation of Molinari et al. (2007), where $E_{\text{iso},53} = E_{\text{iso}}/10^{53}$ erg and E_{iso} is the isotropic energy released in gamma band, $t_{p,2} = t_p/100$ s. With the density of the surrounding medium $n = 10 \text{ cm}^{-3}$, we obtained the initial bulk Lorentz factor $\Gamma \approx 260$, which should be twice of $\Gamma(t_{\text{peak}})$. This number is between the value found by Covino et al. (2008) for GRB 071010A and the value measured by Molinari et al. (2007)

for GRB 060418 and GRB 060607A. With the value of E_{iso} estimated in Section 3, we found that GRB 100219A has a slight bias to the $\Gamma - E_{\text{iso}}$ relation derived by Liang et al. (2010) at the 2σ confidence level. Within the errors, the early bumps shown in the I_C -band and X-ray light curves have the same peak time. However, there are significant differences in the two bumps, e.g., the X-ray flare has a shorter duration and is sharper than the I_C -band bump, suggesting a different origin of these two bumps. The early X-ray bump may be caused by internal activity, as was that of GRB 060418 (Molinari et al. 2007). Furthermore, the smooth decay ($\alpha_d = 0.9 \pm 0.2$) of the I_C -band bump is inconsistent with the rapid-decay prediction ($\alpha_d = 2.0$) for the reverse shock emission (Kobayashi & Zhang 2007). Finally, we remark that the fitting of the early optical bump cannot be accurate, because the I_C -band light curve is poorly sampled and we do not have enough data points with accurate calibration. In the following we focus on the late achromatic bumps shown in the X-ray and optical light curves.

We can calculate the ratio between the duration Δt and the peak time t_p of each bump from our light curve fits to identify the origin of the simultaneous bumps shown in the GRB 100219A afterglow. We converted the time duration as computed in our parametrization to the full-width-at-half-maximum (FWHM) of the bump. We obtained $(\Delta t_{\text{FWHM}}/t_p)_{\text{X},1} = 0.17 \pm 0.26$ for the first X-ray bump, $(\Delta t_{\text{FWHM}}/t_p)_{\text{X},2} = 0.66 \pm 0.57$ for the second X-ray bump and $(\Delta t_{\text{FWHM}}/t_p)_{\text{O}} = 1.46 \pm 0.58$ for the late optical bump. These results can be compared with the predictions by Lazzati & Perna et al. (2007). As illustrated in Fig. 2 of their paper, external shock models predict $\Delta t_{\text{FWHM}}/t_p \geq 2$. It seems that our X-ray and optical rebrightening bumps do not favor an external origin. Instead, within the internal framework, if the flare activity is caused by a freely expanding flow during the prompt phase, the prediction $\Delta t_{\text{FWHM}}/t_p \geq 0.25$ agrees with the observed late X-ray and optical bumps of GRB 100219A. The shorter $\Delta t_{\text{FWHM}}/t_p$ of the first early and sharp X-ray flare at 1000 s indicates that the central engine was active for a time significantly longer than the prompt duration T_{90} . This ejection mechanism has also been proposed by Ghisellini et al. (2007). Therefore, we suggest that the bumps/flares of GRB 100219A have an internal origin from a long-lasting activity of the central engine.

Another model discussed in the literature to interpret rebrightenings is the off-axis jet. The bulk Lorentz factor and the energy per solid angle have in this case some dependency as a function of the off-axis angle (Mészáros et al. 1998). Therefore, the presence of an off-axis jet may modify the temporal power-law decay and produce a smooth bump (Zhang & Mészáros 2002; Kumar & Granot 2003). In the special case of GRB 100219A, we considered the possibility proposed by De Pasquale et al. (2009): a narrow inner jet is responsible for the X-ray emission while the wide outside jet is responsible for the optical emission. Therefore, we speculate that the optical bump has much less off-axis effect than the X-ray bump. Consequently, the optical bump is wider and the inner X-ray flare is narrower. Unfortunately, in our case, we do not observe a clear jet-break either in the X-ray or the optical light curves. This lack of jet-break observation prevents any further analysis.

Finally, from the X-ray analysis, we suggest that the surrounding medium of GRB 100219A might be relatively dense. The neutral hydrogen column density $1.1 \times 10^{22} \text{ cm}^{-2}$ measured in the time-averaged X-ray spectrum at $z \sim 4.7$ is higher than the average value $7.9 \times 10^{21} \text{ cm}^{-2}$ given by the statistics of Campana et al. (2010). Zheng et al. (2009) and Campana et al. (2010) have suggested that the GRB X-ray absorption is intrinsic in general. GRB 100219A shows a “dark” property according to the crite-

tion $\beta_{\text{OX}} \leq 0.5$ introduced by Jakobsson et al. (2004a). However, the low β_{OX} value in the *R*-band is caused by the $\text{Ly}\alpha$ blanketing because this burst is at redshift 4.7. Considering the *I*-band observation, which is not affected by the $\text{Ly}\alpha$ forest, however, $\beta_{\text{OX}} = 0.56$, which is above the criterion by Jakobsson et al. (2004a). By examining the broad-band SED, we can see that the *I*-band data point lies (slightly) below the extrapolation of the X-ray spectrum. This suggests that some flux suppression could be present in the optical, likely caused by dust, although its significance is not high. The high metal column density measured in the X-ray spectrum would suggest a far higher extinction assuming the Galactic dust-to-metal ratio (Mao 2010). A similar mismatch has been noted by many authors and is a general feature of GRB afterglows (e.g., Galama & Wijers 2001; Zafar et al. 2011).

From the above analysis, we caution that (1) the X-ray flare sample selected by Chincarini et al. (2010) is prominently constituted by bright flares, with a peak count rate above 1 count s^{-1} , while in our X-ray light curve, the peaks of the two bumps are lower than this value; this faint feature is therefore hard to model accurately; (2) for the discussion of the late optical bump, we have no data points around the peak time, so that we cannot fully characterize the bump profile; (3) the lack of a jet-break detection prevents us from carrying out a more detailed analysis; (4) as this burst occurred at redshift 4.7, in the optical band, we have only *I*-band observations that are not affected by the $\text{Ly}\alpha$ absorption, consequently, the optical-to-X-ray SED cannot be constructed accurately; (5) although the temporal variabilities can be related to the central engine and jet structure (see Ioka et al. 2005 for a general description and one application to GRB 080210 by De Cia et al. 2011), the explanation of small flares/bumps shown in the GRB light curves is not universal. For example, the optical wiggles of GRB 011211 may be the result of spherically asymmetric density or energy variations (Jakobsson et al. 2004b).

5. Conclusions

We have presented the multi-wavelength observations of GRB 100219A using the data from *Swift* and ground-based telescopes. The early (1000 s) and late (2×10^4 s) achromatic bumps visible in the X-ray and optical light curves are comprehensively discussed. In our analysis, we speculate that the early optical I_C -band bump is probably caused by the afterglow onset while the X-ray one might be caused by the internal activity. The late X-ray and optical bumps may be produced by the internal shell ejection from the long-active central engine. The jet structure could also play an important role for the achromatic property of the bumps. Moreover, the medium surrounding this GRB might be dense.

At present, many theoretical models have been proposed successfully to solve the problems of GRB energy release and to explain some major observational phenomena (such as prompt emission, early X-ray light curve and X-ray flares). However, it is still difficult to simply apply these models to specify the late achromatic bumps discussed in this paper. From this point of view, the theoretical explanations have to concentrate on more subtle observational features in the future.

Acknowledgements. We thank the referee, Elena Pian, for the constructive suggestions and a detailed review. This work made use of XRT data supplied by the UK *Swift* Science Data Centre at the University of Leicester. We thank S. Campana for the discussion of X-ray spectrum. J. Bai, S. Li and J. Mao are financially supported by Natural Science Foundation of China (NSFC, Grant 10973034) and the 973 Program (Grant 2009CB824800). The Dark Cosmology Centre is funded by the Danish National Research Foundation.

References

- Afonso, P., et al. 2011, *A&A*, 526, A154
 Amati, L. 2002, *A&A*, 390, 81
 Amati, L. 2006, *MNRAS*, 372, 233
 Antonelli, L. A., Testa, V., Romano, P., et al. 2006, *A&A*, 456, 509
 Baumgartner, W. H., Barthelmy, S. D., Cummings, J. R., et al. 2010, *GCN Circ.* 10434
 Bernardini, M. G., Margutti, R., Chincarini, G., Guidorzi, C., Mao, J. 2011, *A&A*, 526, 27
 Bertin, E. & Arnouts, S. 1996, *A&AS*, 117, 393
 Bloom, J. S. & Nugent, P. E. 2010, *GCN Circ.* 10433
 Campana, S., Thöne, C. C., de Ugarte Postigo, A., Tagliaferri, G., Moretti, A. & Covino, S. 2010, *MNRAS*, 402, 2429
 Cenko, S. B., et al. 2009, *ApJ*, 693, 1484
 Cenko, S. B., Bloom, J. S., Perley, D. A., & Cobb, B. E. 2010, *GCN circ.* 10443
 Chincarini, G., Moretti, A., Romano, P., et al. 2007, *ApJ*, 671, 1903
 Chincarini, G., Mao, J., Margutti, R., et al. 2010, *MNRAS*, 406, 2113
 Covino, S., D'Avanzo, P., Klotz, A., et al. 2008, *MNRAS*, 388, 347
 Curran, P. A., Starling, R. L. C., O'Brien, P. T., Godet, O., van der Horst, A. J. & Wijers, R. A. M. J. 2008, *A&A*, 487, 533
 De Cia, A., Jakobsson, P., Björnsson, G., et al. 2011, *MNRAS*, 412, 2229
 De Pasquale, M., Evans, P., Oates, S., et al. 2009, *MNRAS*, 392, 153
 De Ugarte Postigo, A., Thoene, C. C., Vergani, S. D., Milvang-Jensen, B., & Fynbo, J. 2010, *GCN circ.* 10445
 Evans, P., Beardmore, A. P., Page, K. L., et al. 2007, *A&A*, 469, 379
 Evans, P., Beardmore, A. P., Page, K. L., et al. 2009, *MNRAS*, 397, 1177
 Evans, P., Goad, M. R., Osborne, J. P., & Beardmore, A. P. 2010, *GCN circ.* 10437
 Fan, Y.-Z., Zhang, B. & Wei, D. M. 2005, *ApJ*, 628, L25
 Frail, D. A., Kulkarni, S. R., Djorgovski, S. G., et al. 2001, *ApJ*, 562, L55
 Galama, T. J. & Wijers, R. A. M. J. 2001, *ApJ*, 549, 209
 Ghisellini, G., Ghirlanda, G., Nava, L. & Firmani, C. 2007, *ApJ*, 658, L75
 Groot, P., Kaper, L., Ellerbroek, L., et al. 2010, *GCN circ.* 10441
 Guidorzi, C., Vergani, S. D., Sazonov, S., et al. 2007, *A&A*, 474, 793
 Holland, S. T., Weidinger, M., Fynbo, J. P. U., et al. 2003, *AJ*, 125, 2291
 Holland, S. T., Kuin, N. P. M., & Rowlinson, A. 2010, *GCN circ.* 10432
 Holland, S. T., & Rowlinson, A. 2010, *GCN circ.* 10436
 Ioka, K., Kobayashi, S., & Zhang, B. 2010, *ApJ*, 631, 429
 Jakobsson, P., Hjorth, J., Fynbo, J. P. U., Watson, D., Pedersen, K., Björnsson, G., Gorosabel, J. 2004a, *ApJ*, 617, L21
 Jakobsson, P., Hjorth, J., Ramirez-Ruiz, E., et al. 2004b, *New Astronomy*, 9, 435
 Jakobsson, P., Malesani, D., Villforth, C., Hjorth, J., Watson, D. J., & N. R. Tanvir, N. R. 2010, *GCN circ.* 10438
 Kinugasa, K., Honda, S., Takahashi, H., Taguchi, H., & Hashimoto, O. 2010, *GCN Circ.* 10452
 Klotz, A., Gendre, B., Stratta, G., et al. 2008, *A&A*, 483, 847
 Klotz, A., Boer, M., Atteia, J. L., & Gendre, B. 2009, *AJ*, 137, 4100
 Kobayashi, S., & Zhang, B. 2007, *ApJ*, 655, 973
 Krühler, T., Greiner, J., McBreen, S., et al. 2009, *ApJ*, 697, 758
 Kruehler, T., Nicuesa, A., Klose, S., Greiner, J., & Afonso, P. 2010, *GCN circ.* 10439
 Kumar, P. & Granot, J. 2003, *ApJ*, 591, 1075
 Kuroda, D., Yanagisawa, K., Shimizu, Y., et al. 2010, *GCN circ.* 10440
 Landolt, A. U. 1992, *AJ*, 104, 340
 Lazzati, D., Rossi, E., Covino, S., Ghisellini, G., & Malesani, D. 2002, *A&A*, 396, L5
 Lazzati, D. & Perna, R. 2007, *MNRAS*, 375, L46
 Liang, E.-W., Yi, S.-X., Zhang, J., et al. 2010, *ApJ*, 725, 2209
 Malesani, D., Covino, S., D'Avanzo, P., et al. 2007, *A&A*, 473, 77
 Mao, J. 2010, *ApJ*, 717, 140
 Mészáros, P., Rees, M. J. & Wijers, R. A. M. J. 1998, *ApJ*, 499, 301
 Melandri, A., Mundell, C. G., Kobayashi, S., et al. 2008, *ApJ*, 686, 1209
 Melandri, A., Kobayashi, S., Mundell, C. G., et al. 2010, *ApJ*, 723, 1331
 Molinari, E., Vergani, S. D., Malesani, D., et al. 2007, *A&A*, 469, L13
 Mundell, C. G., Melandri, A., Guidorzi, C., et al. 2007, *ApJ*, 660, 489
 Nakar, E., Piran, T., & Granot, J. 2003, *NewA*, 8, 495
 Norris, J. P., Bonnell, J. T., Kazanas, D., Scargle, J. D., Hakkila, J., Giblin, T. W. 2005, *ApJ*, 627, 324
 Nousek, J. A., Kouveliotou, C., Grupe, D., et al. 2006, *ApJ*, 642, 389
 Oates, S. R., Page, M. J., Schady, P., et al. 2009, *MNRAS*, 395, 490
 Panaitescu, A., Mészáros, P., Burrows, D., Nousek, J., Gehrels, N., O'Brien, P. & Willingale, R. 2006, *MNRAS*, 369, 2059
 Perri, M., Guetta, D. & Antonelli, L. A., et al. 2007, *A&A*, 471, 83
 Rees, M. J. & Mészáros, P. 1998, *ApJ*, 496, L1
 Roming, P. W. A., Vanden Berk, D., Pal'shin, V., et al. 2006, *ApJ*, 651, 985
 Rowlinson, A., Barthelmy, S. D., Baumgartner, W. H., et al. 2010, *GCN Circ.* 10430

- Rowlinson, A. 2010, GCN Circ. 10444
- Rykoff, E. S., Aharonian, F., Akerlof, C. W., et al. 2009, *ApJ*, 702, 489
- Sakamoto, T., Sato, G., Barbier, L., et al. 2009, *ApJ*, 693, 922
- Sari, R., Piran, T., & Narayan, R. 1998, *ApJ*, 497, L17
- Stetson, P. B. 1987, *PASP*, 99, 191
- Thöne, C., et al. 2011, *A&A*, submitted
- Uehara, T., Uemura, M., Kawabata, K. S., et al. 2010, *A&A*, astro/1006.0785
- Yost, S. A., Harrison, F. A., Sari, R., Frail, D. A. 2003, *ApJ*, 597, 459
- Zacharias, N. 1997, *AJ*, 113, 1925
- Zafar, T., Watson, D., Fynbo, J. P. U., Malesani, D., Jakobsson, P., & de Ugarte Postigo, A. 2011, *A&A*, 532, 143
- Zhang, B. & Mészáros, P. 2002, *ApJ*, 571, 876
- Zhang, B., Kobayashi, S. & Mészáros, P. 2003, *ApJ*, 595, 950
- Zhang, B., Fan, Y. Z., Dyks, J., Kobayashi, S., Mészáros, P., Burrows, D. A., Nousek, J. A. & Gehrels, N. 2006, *ApJ*, 642, 354
- Zheng, W., Deng, J. & Wang, J. 2009, *Research of Astronomy and Astrophysics*, 9, 1103